2614 *Inorg. Chem.* **2010**, *49*, 2614–2623
DOI: 10.1021/ic901421m

Inorganic Chemistry
Article

Syntheses, Characterization, and Photophysical Properties of Conjugated Organometallic Pt-Acetylide/Zn(II) Porphyrin-Containing Oligomers

Feng-Lei Jiang, Daniel Fortin, and Pierre D. Harvey*

Département de Chimie, Université de Sherbrooke, PQ, Canada J1K 2R1

Received July 21, 2009

Two conjugated organometallic oligomers of the type $(-C{\equiv}CPt(L)_2C{\equiv}C(Zn\mathbf{P})-)_n$ and model compounds [PhC≡CPt(L)$_2$C≡C(Zn**P**)C≡CPt(L)$_2$C≡CPh] with L = tri(*n*-butyl)-phosphine and Zn**P** = zinc(II)(10,20-bis(Ar)porphyrine) (Ar = mesityl (Mes; **P1** and **M1**) or 3,4,5-trihexadecyloxyphenyl (**P2** and **M2**)) were synthesized and characterized (^{1}H and ^{31}P NMR, HRMS, elemental analysis, IR, GPC, and TGA). GPC indicates that **P1** and **P2** exhibit respectively ∼6 and ∼3 units with a polydispersity of 1.4. **M1** was also characterized by X-ray crystallography. The Pt···Pt separation in **M1** is 1.61 nm, which makes **P1** ∼ 9.6 nm long. The spectral measurements show that the absorption and photoluminescence spectra of **M1**, **M2**, **P1**, and **P2** are remarkably red-shifted. For example, the low energy Q-band is observed at 677 ± 1 nm in comparison with their precursors HC≡C(Zn**P**)C≡CH, **L1** and **L2** (Ar=mesityl (Mes; **L1**) or 3,4,5-trihexadecyloxyphenyl (**L2**)), both at 298 and 77 K, for which the Q-band is observed at 622 nm. The photophysical parameters, fluorescence lifetimes (τ_F), and quantum yields (Φ_F) show a slight decrease by a factor of 2 (at most 3) following the trend **L1** ∼ **L2** > **M1** ∼ **M2** > **P1** ∼ **P2**, a trend explained by a combination of the heavy atom effect and an increase in internal conversion rate due to the increase in oligomer dimension. This small variation of the photophysical data for materials of a few nm in dimension contrasts with the larger change in τ_P, phosphorescence lifetimes of the Pt-containing unit in the $(-C_6H_4C{\equiv}CPt(L)_2C{\equiv}C-CC_6H_4(Zn\mathbf{P})-)_n$ oligomers with n = 3, 6, and 9 reported earlier (Liu, L.; Fortin, D.; Harvey, P. D. *Inorg. Chem.* **2009**, *48*, 5891−5900). In this later case, τ_P decreased by steps of an order of magnitude as n increased from 3 to 6 to 9. This decrease was explained by a T_1 energy transfer from the Pt unit (donor) to M**P** (acceptor) in combination with an excitonic process (energy delocalization). Because of the full conjugation in **P1** and **P2**, these oligomers behave as distinct molecules, and no energy transfer occurs. These properties make these materials suitable candidates for photocell applications.

Introduction

In recent years, great attention was paid to the metallopolyyne polymers expected for applications in optoelectronics such as light-emitting diodes (LEDs) and photovoltaic cells.[1] Indeed, the incorporation of a transition metal into macromolecular organic scaffolds can lead to hybridization of the electronic, optical, and magnetic properties of metal complexes with the solubility and processability of carbon-based polymers. Researchers focused primarily on transition metal, notably Pt(II), acetylide oligoynes and polyynes containing repeated units like *trans*-$[-M(L)_2C{\equiv}C(R)C{\equiv}C-]_n$, where M is inserted in the macromolecules, L is an auxiliary ligand, and R is a spacer unit, most of the time an aromatic residue. Owing to the spin−orbit coupling caused by the presence of heavy metals, the spin-forbidden triplet emission with a longer lifetime is partially allowed, which is advantageous for LEDs. The ultimate efficiency of LEDs is largely controlled by the fraction of triplet states generated or harvested since spin statistics suggest a ratio of 3:1 for the generation of a nonemissive triplet to emissive singlet exciton.[2] Recent progress has shown that metal-containing complexes should, in principle, be superior to fluorescent substrates for small-molecule organic LED applications.[1c,2]

The photovoltaic application of metallopolyynes has been largely hampered by their wide bandgaps (E_g), and most of the Pt(II) polyynes compare unfavorably with those of some conjugated organic polymers comprising alternating electron donor and acceptor units.[3] Hence, new synthetic strategies for creating metallopolyynes of low E_g would be desirable. According to the energy gap law for triplet emission, the nonradiative decay rate from the triplet state increases exponentially with the decreasing triplet−singlet energy gap (ΔE_{S-T}).[4] A concise

*To whom correspondence should be addressed. Tel: 1-819-821-7092. Fax: 1-819-821-8017. E-mail: Pierre.harvey@usherbrooke.ca.

(1) (a) Wong, W.-Y. *Dalton Trans.* **2007**, 4495–4510. (b) Wong, W.-Y.; Ho, C.-L. *Coord. Chem. Rev.* **2006**, *250*, 2627−2690 and references therein. (c) Wong, W.-Y.; Harvey, P. D. *Macromol. Rapid Commun.* **2010**, in press.

(2) Cleave, V.; Yahioglu, G.; Le Barny, P.; Friend, R. H.; Tessler, N. *Adv. Mater.* **1999**, *11*, 285–288.

(3) Roncali, J. *Chem. Rev.* **1997**, *97*, 173–206.

(4) Wilson, J. S.; Chawdhury, N.; Al-Mandhary, M. R. A.; Younus, M.; Khan, S. M.; Raithby, P. R.; Köhler, A.; Friend, R. H. *J. Am. Chem. Soc.* **2001**, *123*, 9412–9417.

Published on Web 02/08/2010

Chart 1

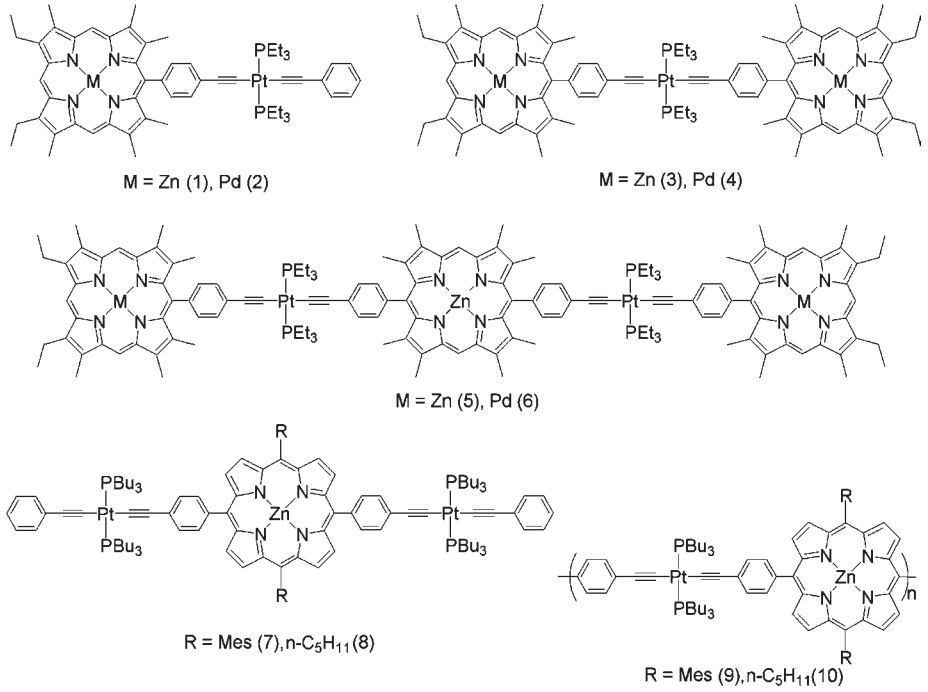

consideration and a good compromise of the triplet photophysics and the associated E_g in the polymer are essential in the design of highly efficient and wavelength-tunable luminescent and photovoltaically active materials.

Porphyrin monomers have a relatively low E_g with large absorption coefficients due to their large π conjugation. Even larger π conjugation in porphyrin oligomers and polymers results in an even lower E_g and larger absorption coefficients in the red-shifted Q-band.[5] Many researchers focused on porphyrin oligomers and polymers bridged by ethyne,[5] butadiyne,[6] phenylenevinylene,[7] aryl acetylene,[8] etc., which were mostly studied for their nonlinear optical properties,[6a−f] electron transfer,[6g] single molecule conductance with ultra low attenuation,[6h,i] and functionalization and solubilization of the carbon nanotubes.[6j] However, there are very few conjugated porphyrin oligomers bridged by Pt(II) acetylides, except for a report on a porphyrin oligomer bridged by bis(phosphine)platinum(II),[9] in which the monomers are cationic with no definite chemical composition and the monomers and oligomers are mainly investigated for their morphology rather than photophysical properties.[10] Besides the heavy metal effect, insertion of Pt(II) in macromolecules also led to a large conduction bandwidth with a d^8 square-planar configuration.[11] In connection with this class of compounds and polymers, we recently reported a series of well-defined short oligomers containing the fragments $[C_6H_4C{\equiv}CPtL_2C{\equiv}CC_6H_4]$ (L = monophosphine) and metallophorphyrins (**MP**; see compounds **1**−**6**)[12a] as well as longer poly-dispersed oligomers (see compounds **7** and **8**, and polymers **9** and **10** in Chart 1).[12b]

In these studies on alternating nonconjugated and partially conjugated $(A-B)_n$ materials, the T_1 energy transfer processes between the $[C_6H_4C{\equiv}CPtL_2C{\equiv}CC_6H_4]$ spacer (donor in black) and **MP** (acceptor in gray) as well as the S_1 and T_1 energy transfers between the **MP** (M = Pd, donor; M = Zn, acceptor) were observed (Scheme 1). These results illustrated that the spacer and the metalloporphyrin moieties act as distinct chromophores. Moreover, the main conclusion is that the rates for T_1 energy transfers are slow (on the order of 10^4 s^{-1}) but vary as the oligomer length gets longer.[12b] In fact, in the series **8** and **10** (where n = 3, 6, 9), the rate increases by an order of magnitude when n passes from 3 (10^4) to 6 (10^5) to 9 (10^6 s^{-1}). This indicates that an excitonic process

(5) Duncan, T. V.; Susumu, K.; Sinks, L. E.; Therien, M. J. *J. Am. Chem. Soc*. **2006**, *128*, 9000–9001.

(6) (a) Anderson, H. L.; Martin, S. J.; Bradley, D. D. C. *Angew. Chem., Int. Ed. Engl*. **1994**, *33*, 655–657. (b) Taylor, P. N.; Huuskonen, J.; Rumbles, G.; Aplin, R. T.; Williams, E.; Anderson, H. L. *Chem. Commun*. **1998**, 909–910. (c) Anderson, H. L. *Chem. Commun*. **1999**, 2323–2330. (d) Kuebler, S. M.; Denning, R. G.; Anderson, H. L. *J. Am. Chem. Soc*. **2000**, *122*, 339–347. (e) Screen, T. E. O.; Thorne, J. R. G.; Denning, R. G.; Bucknall, D. G.; Anderson, H. L. *J. Mater. Chem*. **2003**, *13*, 2796–2808. (f) Drobizhev, M.; Stepanenko, Y.; Rebane, A.; Wilson, C. J.; Screen, T. E. O.; Anderson, H. L. *J. Am. Chem. Soc*. **2006**, *128*, 12432–12433. (g) Winters, M. U.; Dahlstedt, E.; Blades, H. E.; Wilson, C. J.; Frampton, M. J.; Anderson, H. L.; Albinsson, B. *J. Am. Chem. Soc*. **2007**, *129*, 4291–4297. (h) Sedghi, G.; Sawada, K.; Esdaile, L. J.; Hoffmann, M.; Anderson, H. L.; Bethell, D.; Haiss, W.; Higgins, S. J.; Nichols, R. J. *J. Am. Chem. Soc*. **2008**, *130*, 8582–8583. (i) Meier, H. *Angew. Chem., Int. Ed*. **2009**, *48*, 3911–3913. (j) Adronov, A.; Cheng, F. *Chem.—Eur. J*. **2006**, *12*, 5053–5059.

(7) (a) Jiang, B.; Yang, S.-W.; Jones, W. E., Jr. *Chem. Mater*. **1997**, *9*, 2031–2034. (b) Jiang, B.; Jones, W. E., Jr. *Macromolecules* **1997**, *30*, 5575–5581.

(8) (a) Jiang, B.; Yang, S.-W.; Barbini, D. C.; Jones, W. E., Jr. *Chem. Commun*. **1998**, 213–214. (b) Li, B.; Fu, Y.; Han, Y.; Bo, Z. *Macromol. Rapid Commun*. **2006**, *27*, 1355–1361. (c) Screen, T. E. O.; Lawton, K. B.; Wilson, G. S.; Dolney, N.; Ispasoiu, R.; Goodson, T., III; Martin, S. J.; Bradley, D. D. C.; Anderson, H. L. *J. Mater. Chem*. **2001**, *11*, 312–320.

(9) Ferri, A.; Polzonetti, G.; Licoccia, S.; Paolesse, R.; Favretto, D.; Traldi, P.; Russo, M. V. *J. Chem. Soc., Dalton Trans*. **1998**, 4063–4069.

(10) (a) Amato, M. E.; Licciardello, A.; Torrisi, V.; Ugo, L.; Venditti, I.; Russo, M. V. *Mater. Sci. Eng., C* **2009**, *29*, 1010–1017. (b) Fratoddi, I.; Battocchio, C.; Amato, R. D.; Di Egidio, G. P.; Ugo, L.; Polzonetti, G.; Russo, M. V. *Mater. Sci. Eng., C* **2003**, *23*, 867–871.

(11) Flapper, G.; Kertesz, M. *Inorg. Chem*. **1993**, *32*, 732–740.

(12) (a) Bellows, D.; Aly, S. A.; Gros, C. P.; Ojaimi, M. E.; Barbe, J.-M.; Guilard, R.; Harvey, P. D. *Inorg. Chem*. **2009**, *48*, 7613–7629. (b) Liu, L.; Fortin, D.; Harvey, P. D. *Inorg. Chem*. **2009**, *48*, 5891–5900.

Scheme 1. Non-Radiative Energy Delocalization Processes in Pt-Acetylides/Porphyrin Oligomers

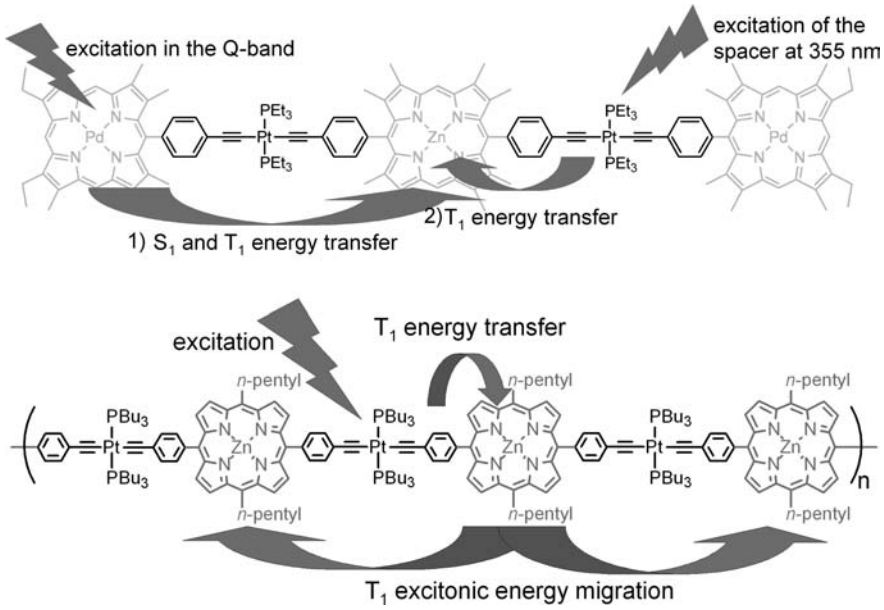

Chart 2

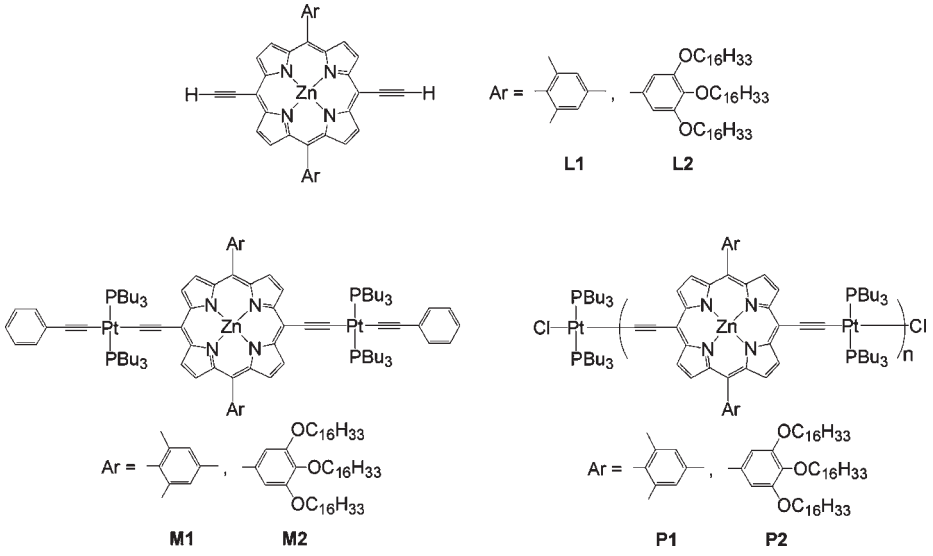

(i.e., energy delocalization) takes place along the backbone of the oligomers when the number of acceptor units increases (lesser probability of back energy transfer), hence accelerating the T_1 energy transfer between the donor and the acceptor. Nonetheless, the rate is still slow. The next question is, what does it take to accelerate the rates? One possible answer is to render the $(A-B)_n$ polymers fully conjugated, so the electronic communication between the chromophores A and B is improved with respect to the previous systems. Then, the next obvious question is, what is the role of the oligomer length in the photophysical properties when the system is totally conjugated?

We now wish to report herein the synthesis, characterization, photophysical properties, density functional theory (DFT), and time dependent density functional theory (TDDFT) analyses of porphyrin monomers (as model compounds) and oligomers bridged by Pt(II) acetylides (Chart 2).

Results and Discussion

Synthesis and Characterization. The starting materials, Zn(II)[5,15-bis(mesityl)-10,20-bis(ethynyl)porphyrinate] (**L1**) and Zn(II)[5,15-bis[3,4,5-tri(hexadecyloxy)phenyl]-10,20-bis(ethynyl)porphyrinate] (**L2**), were prepared according to the literature.[8a,6j] The reaction of **L1** or **L2** with two equivalents of *trans*-chloro(ethynylbenzene)bis(tris-*n*-butylphosphine)platinum(II) in the presence of CuI in CH_2Cl_2 and iPr_2NH (v/v, 1:1) gave the model compounds **M1** and **M2** in 44−47% yield, while the same workup in the reaction of **L1** and **L2** with *trans*-[Pt(P-*n*-$Bu_3)_2Cl_2$] gave plastic like materials for porphyrin oligomers **P1** and **P2** in about 60% yield. **M1** and **M2** are characterized by ^1H and ^{31}P NMR, MALDI-TOF high resolution mass spectrometry (HRMS), FT-IR, and thermal gravity analysis (TGA), each of which proves their molecular structures, shown in Scheme 2.

Scheme 2. Synthetic Route for **M1**, **M2**, **P1**, and **P2**

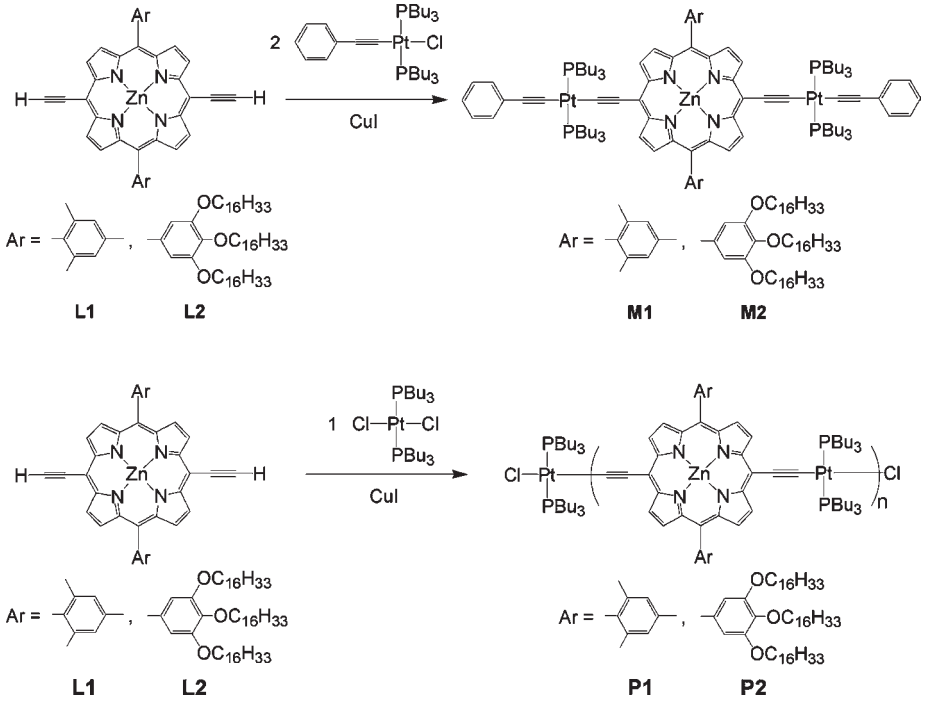

Taking **M1**, for example, two doublets at 9.59 and 8.52 ppm with the same *J*-coupling of 6.1 Hz in the proton NMR of **M1** are assigned to the protons at the β positions of the pyrrole unit of the porphyrin macrocycle. These two doublets confirm the symmetrical chemical structure. Two singlets at 2.66 and 1.87 ppm are ascribed to the mesityl group with an integration intensity ratio of 1:2. The combination of a Pt(II) moiety with a porphyrin moiety is ascertained by four multiplets in the region 2.34−0.89 ppm, which are assigned to pendant *n*-butyl groups. In ^{31}P NMR, the chemical shift of phosphorus is shown at 5.87 ppm with two satellite peaks giving a *J*-coupling $^{1}J_{\mathrm{Pt-P}} = 3100$ Hz which further proves the symmetrical conformation of this compound. A peak at *m*/*z* 2057.799 shown in MALDI-TOF-HRMS is the M^+ ion with a deviation of less than 1 ppm. The FT-IR spectrum shows no band at 3300 cm^{-1} (≡C−H stretching vibration), while the band at 2080 cm^{-1} (C≡C stretching vibration) further reveals the successful coordination of the Pt(II) moiety onto the porphyrin-containing ligands **L1** and **L2**. Thermal gravity analysis shows **M1** and **M2** are thermally stable with $T_{10\%\mathrm{decomp}}$ (temperature when 10% of the compound is decomposed) = 328 and 300 °C, respectively. Owing to the long hexadecyl group, it is easier for **M2** to lose methyl and other alkyl groups. **M1** and **M2** are both air-stable and soluble in common solvents such as chloroform, dichloromethane, and tetrahydrofuran (THF), for example, but **M2** is more soluble than **M1** due to its long side chains.

In order to reduce the polydispersity of the two porphyrin oligomers, different purification methods were attempted. **P2** is readily soluble in common solvents; hence flash column chromatography on silica gel can be performed. Better results are obtained when the solution of **P2** was dissolved in a minimum of dichloromethane and methanol was added to induce a precipitation of **P2** with a polydispersity of 1.43. However, **P1** exhibits a low

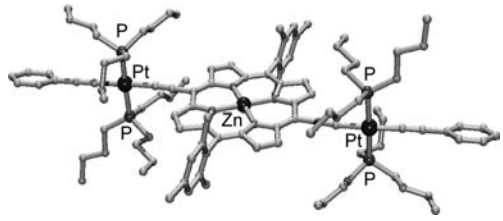

Figure 1. X-ray structure of **M1**. Hydrogen atoms are omitted for clarity.

solubility in chlorinated solvents, and therefore it was washed with dichloromethane to remove the unreacted starting materials. At last, a polydispersity of 1.41 was obtained for **P1**. Despite its poor solubility, **P1** can be dissolved in 2-MeTHF in order to carry out all the photophysical measurements. The GPC results, using polystyrene as a standard and THF as the solvent, indicate that the number-average molecular weights M_n for **P1** and **P2** are 7307 and 8349, respectively. Although it was reported that the starting material **L2** gave a M_n value of 3250 (higher than the theoretical value of 2016.51) caused by overestimation of the molecular weight of rigid-rod polymers with polystyrene as a standard,[6j] the M_n of **L2** is 1917 similar with its theoretical value obtained from GPC. From this analysis, the approximate number of repeated units for **P1** and **P2** is 5.8 and 3.2, respectively. The higher degree of polymerization for **P1** versus that for **P2** may lay in the chemical structures since **L2** is much more bulky than **L1**, as it has several long alkyl chains at its *meso* positions. This feature makes it harder for reactants to interact. Attempts were made to obtain higher degrees of polymerization for both oligomers using higher reaction temperatures but failed when the temperature was higher than 65 °C. The peaks in ^{1}H NMR spectra of **P1** and **P2** are all broadened (except for those assigned to

Table 1. Photophysical Data for **L1**, **L2**, **M1**, **M2**, **P1**, and **P2** in 2-MeTHF at 298 and 77 K[a]

		excitation (nm)		emission (nm)[b]		quantum yield[c]		emission lifetimes[d]	
	λ_{max} (nm) ($\varepsilon \times 10^{-4}M^{-1}cm^{-1}$)	298 K	77 K	298 K	77 K	298 K	77 K	298 K	77 K
L1	432 (21.2), 442 (16.0), 576 (1.83), 622 (2.27)	432, 442	435, 447	626, 684	630, 687	0.14	0.14	2.37 ± 0.08 ns	3.13 ± 0.08 ns
L2	434 (28.2), 444 (25.2), 574 (2.14), 622 (2.62)	434, 444	438, 452	629, 685	636, 701	0.068	0.012	1.93 ± 0.08 ns	0.19 ± 0.08 ns
M1	314 (11.4), 456 (66.3), 606 (3.93), 658 (13.0)	456	337, 456	669, 742	437, 669, 745	0.082	0.011	0.46 ± 0.08 ns	32.6 ± 1.1 μs [Pt][e]; 0.54 ± 0.08 ns
M2	316 (11.8), 456 (47.3), 606 (4.46), 658 (10.6)	456	459	671, 744	683, 759	0.0072	0.0076	0.43 ± 0.08 ns	0.21 ± 0.08 ns
P1	302 (7.72), 466 (23.5), 678 (9.98)	462	461	682, 754	684, 754	0.016	0.0034	0.39 ± 0.08 ns	0.29 ± 0.08 ns
P2	302 (9.26), 462 (25.4), 676 (7.60)	462	463	680, 750	685, 770	0.010	0.0055	0.38 ± 0.08 ns	f

[a] All luminescence measurements at 298 K were performed under an inert atmosphere. The other measurements (absorption and luminescence) were performed without degassing the solutions. [b] The fluorescence lifetimes were measured using λ_{exc} corresponding to the Soret band, and λ_{emi} corresponding to the 0−0 of the fluorescence. [c] The uncertainties are on the order of ±10%. [d] Lifetime decays are measured using λ_{exc} = 437 nm; the decay traces are placed in the SI; the uncertainty on the fluorescence lifetimes is based upon the variation of several measurements. [e] Phosphorescence arising from [Pt] (i.e., (*trans*-Pt(P-*n*-Bu_3)$_2$(C≡C-*p*-C_6H_4)$_2$). [f] Too short to be accurately measured.

n-butyl groups in the range 0.8−2.3, which are sharp) demonstrating the successful coupling between the porphyrin and Pt(II) moiety. This is further confirmed by the FT-IR spectrum in which a band is observed at ca. 2080 cm^{-1} (ν(C≡C)). The ^{31}P NMR signals at 7.57 and 7.82 ppm are also traced for **P1** and **P2**, respectively. We find no signal attributable to the CC−H end group in the ^{1}H spectra, meaning that the end groups in **P1** and **P2** must be the PtL_2Cl residue. Thermal gravity analysis shows the $T_{10\%decomp}$ for **P1** and **P2** are 385 and 312 °C, respectively, which coincides with the trend for **M1** and **M2**.

A single crystal of **M1** suitable for X-ray diffraction was grown by slow evaporation of a mixture of a CH_2Cl_2/MeOH solution at room temperature. The crystal structure is shown in Figure 1, and the crystallographic data are placed in Table S1 of the Supporting Information (SI). The identity of **M1** is of no doubt. The *trans* geometry of the two Pt centers is demonstrated.

Spectroscopic Data, DFT and TDDFT Analyses. All measurements are carried out in 2-MeTHF (Table 1). The absorption spectra of the **L1** and **L2** (see Figure S5 in the SI and refer to Table 1 for peak maxima; typical spectra are also shown below for **P1** and **P2**) exhibit split Soret bands located at 432 and 442 nm and at 434 and 444 nm, respectively. The splitting readily expected for porphyrins of reduced symmetry is corroborated by DFT (B3LYP/6-31G*) and TDDFT computations (B3LYP/6-31G*/THF PCM model) as presented below. After geometry optimization of **L1**, the computed frontier MOs (Figure 2) unambiguously show the π nature of these MOs, hence strongly indicating that the lowest energy transitions and excited states are of the $\pi\pi^*$ type. The computed lowest energy transitions (TDDFT; Table 2) indeed show that the four lowest energy transitions are mixtures of different individual electronic transitions composed of these four same MOs (green lines in Figure 2). The splitting is obvious where a computed 10 nm (experimental 10 nm) is obtained for the Soret band for **L1**. The relative intensity of the two Soret bands is also felt in the oscillator strengths (Osc. Str.). For the Q-band, two electronic transitions are computed and separated by 7 nm. Experimentally, only a weak shoulder is observed for **L1** at 77 K at ∼615 nm, appearing as a weak shoulder beside a stronger 0−0 peak at 623 nm. A peak located at 576 nm is also apparent, but this feature

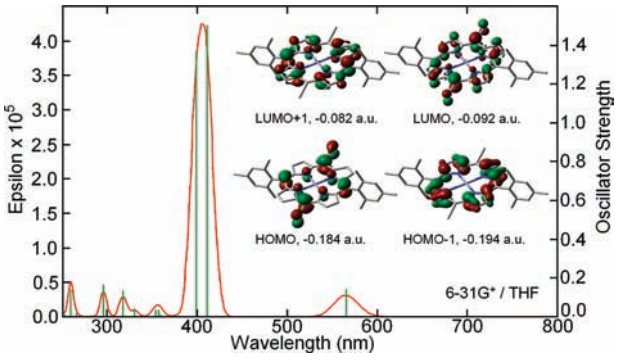

Figure 2. Computed frontier MOs for an optimized geometry of **L1** by DFT, along with the computed pure electronic transitions and generated absorption bands.

Table 2. TDDFT Parameters for the Four First Observable Electronic Transitions for **L1**[a]

no.	ν (cm^{-1})	λ (nm)	osc. str.	major contributions (%)
1	17 700	565	0.1402	H−1→L+1 (31), HOMO→LUMO (66)
2	17 924	558	0.0018	H−1→LUMO (52), HOMO→L+1 (51)
3	24 363	410	1.5022	H−1→LUMO (32), HOMO→L+1 (34)
4	24 520	408	0.0017	H−6→LUMO (97)
5	25 112	398	1.3667	H−1→L+1 (53), HOMO→LUMO (14)

[a] The S_0 optimized geometry was first performed, followed by TDDFT computations using 6-31G* basis sets for Zn, C, H, and N; polarized basis sets for P; and SBKJC and VDZ with effective core potentials for Pt and the THF PCM model.

may be of vibronic origin. A computed spectrum generated by assigning a thickness of each individual transition resembles the experimental (Figure S5, SI, and Table 1) well.

Because the calculated Q-band is 57 nm blue-shifted with respect to the experimental one in **L1**, for example, both the 6-31G* and 3-21G* basis sets were used for Zn, C, H, and N (the rest remains the same), and the THF PCM model was used with all the TDDFT calculations to mimic the 2-MeTHF recorded spectra, for comparison purposes. The results show that the calculated band maxima are more blue-shifted for 3-21G* than for 6-31G* or for 6-31G* coupled to the presence of THF (i.e., PCM THF model). Only the most red-shifted data are placed in the text (because it provides closer calculated data to the experimental

Table 3. TDDFT Parameters for the Four First Observable Electronic Transitions for **M1**[a]

no.	ν (cm^{-1})	λ (nm)	Osc. Str.	Major contributions (%)
1	17 262	579	0.0881	H−2→LUMO (24), HOMO→L+1 (65)
2	17 443	573	0.6136	H−2→L+1 (18), HOMO→LUMO (66)
3	17 948	557	0.0002	H−1→LUMO (95)
4	18 170	550	0	H−1→L+1 (95)
5	23 712	422	0.0175	H−5→LUMO (21), H−4→LUMO (23), H−3→LUMO (42)
6	23 808	420	0.0417	H−6→LUMO(16), H−5→LUMO(15), H−4→LUMO(47) H−3→LUMO (16)
7	24 125	415	1.1066	H−6→LUMO (28), H−5→LUMO (12), H−2→L+1 (30)
8	24 202	413	0.3119	H−5→LUMO (43), H−3→LUMO (31)
9	24 461	409	0.6202	H−4→L+1 (18), H−2→LUMO (45), HOMO→L+1 (10)

[a] The S_0 optimized geometry was first performed, followed by TDDFT computations using 6-31G* basis sets for Zn, C, H, and N; polarized basis sets for P; and SBKJC and VDZ with effective core potentials for Pt and the THF PCM model.

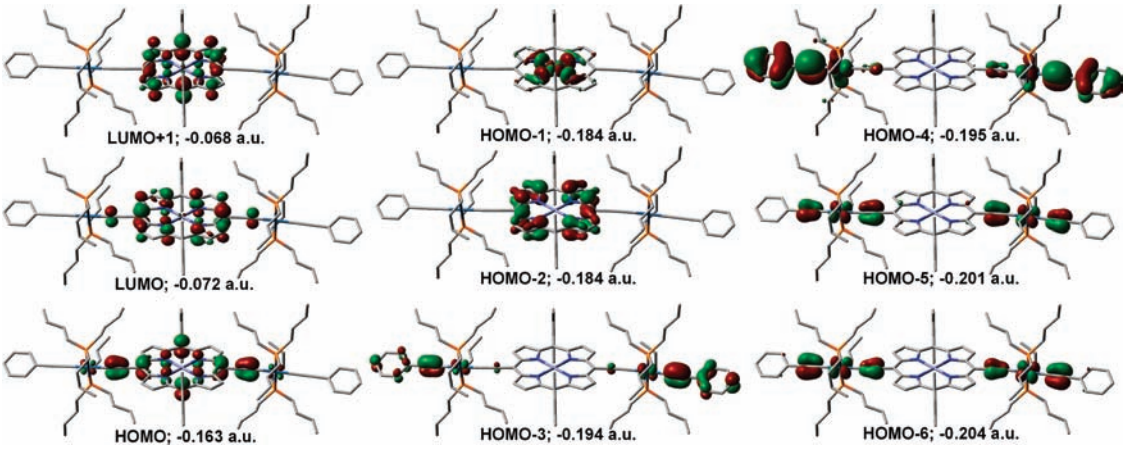

Figure 3. MO representations of the frontier MOs for **M1** (from LUMO+1 to HOMO−6). The geometry of **M1** was optimized first using 6-31G* basis sets for Zn, C, H, and N; polarized basis sets for P; and SBKJC and VDZ with effective core potentials for Pt.

values). The comparison of the calculated spectra and a table for the TDDFT parameters for the first observable electronic transitions for **L1** using the 6-31G* basis set (no THF PCM model added) are placed in the SI. Similar computations and comparisons were made for **M1** and **M2**, described below, and led to the same observation (SI). For **M1** and **M2**, the discrepancy is 79 and 74 nm, respectively, at best with 6-31G* with the PCM THF model. Despite this difference, the conclusions are not affected (i.e., assignment of the nature of the excited states) since these are well-known for porphyrin derivatives.

The chemical coupling of **L1** and **L2** onto two Pt moieties results in the formation of compounds **M1** and **M2**. Both exhibit red-shifted Soret bands at 456 nm (see Figure S6 in the SI) suggesting interactions between the metal atom and the π-system via conjugation. For the square-planar Pt acetylide complexes, it was reported that there are strong interactions between metal dπ orbitals and filled acetylide π orbitals, although no significant metal−ligand back-bonding was found.[13] Previous research indicated that the electronic coupling through an alkyne−Pt−alkyne bridge was only somewhat smaller than through an alkyne−benzene−alkyne bridge, while this case also appeared in this study.[14] The coupling of **L1**

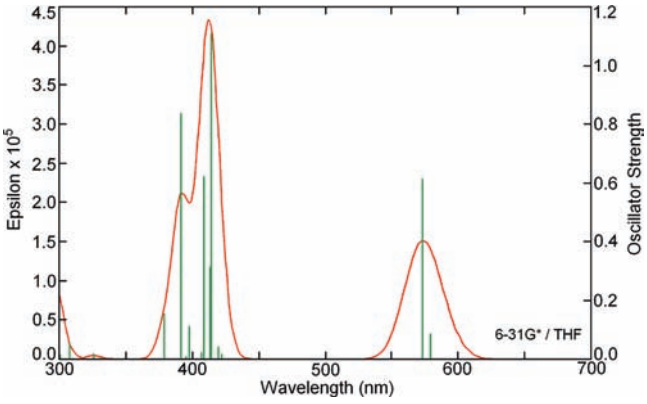

Figure 4. TDDFT computed electronic transitions and generated absorption bands for **M1** using optimized geometries in the S_0 state using 6-31G* basis sets for Zn, C, H, and N; polarized basis sets for P; and SBKJC and VDZ with effective core potentials for Pt and the THF PCM model.

and **L2** with the PtL_2 moiety leads to a material exhibiting red shifts of both the Soret band and Q bands as well as an enhancement of the intensity of Q-band. To corroborate the experimental data, DFT and TDDFT calculations were performed on **M1** using the X-ray structure (Table 3), whereas an optimized geometry for **M2** was used where the $C_{16}H_{33}$ chains were replaced by CH_3 groups to save computation time.

The relevant frontier MOs for **M1** and **M2** are shown in Figure 3 and in Figure S3 in the SI, respectively. Only the description of **M1** will be presented here. It is the same as

(13) (a) Schull, T. L.; Kushmerick, J. G.; Patterson, C. H.; George, C.; Moore, M. H.; Pollack, S. K.; Shashidhar, R. *J. Am. Chem. Soc.* **2003**, *125*, 3202–3203. (b) Louwen, J. N.; Hengelmolen, R.; Grove, D. M.; Oksam, A. *Organometallics* **1984**, *3*, 908–918.

(14) Jones, S. C.; Coropceanu, V.; Barlow, S.; Kinnibrugh, T.; Timofeeva, T.; Brédas, J.-L.; Marder, S. R. *J. Am. Chem. Soc.* **2004**, *126*, 11782–11783.

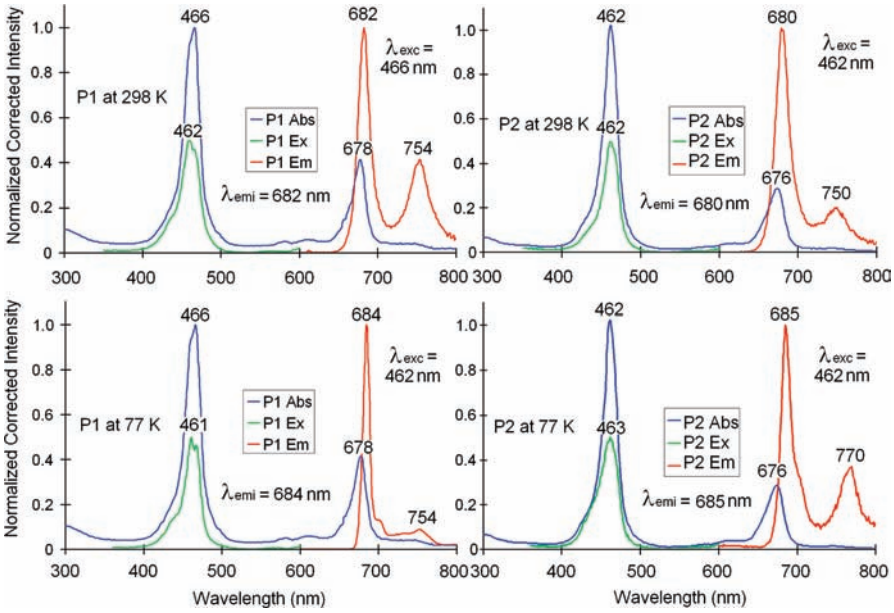

Figure 5. Absorption (blue), excitation (green), and emission spectra (red) of **P1** (left) and **P2** (right) in 2-MeTHF at 298 (top) and 77 K (bottom).

M2. Again, the HOMO, HOMO−1, LUMO, and LUMO+1 are all π systems bearing a strong resemblance with that of **L1**. A minor contribution arising from the Pt d_{xy} orbital is computed for the LUMO+1, hence corroborating evidence for Pt interactions. HOMO−3, −4, −5, and −6 are interesting orbitals since they are specific to the π systems in the −C≡CPh arms present only in **M1** and **M2**. This bears a consequence on the observation of upper energy phosphorescence in **M1**. HOMO−1 is the σ*(Zn−N) orbital accidentally degenerated with HOMO−2.

The overall generated gas phase spectra for **M1** and **M2** (similar to the red line shown in Figure 2) resembles the experimental ones (see Figure S2, Table S4 in the SI). The major difference is that more bands in the Q and Soret regions are computed (Figure 4). The key feature is that the Soret region is composed of 4 calculated transitions, three of them involving HOMO−3 and HOMO−6, predicting the Soret band to exhibit a strong charge transfer character from the C≡CPtC≡C unit to the M**P** moiety along with the $\pi\pi$* transition. This is indeed consistent with the increase in absorptivity experimentally observed for **M1** and **M2** (Table 1). However, the major contribution of this transition is HOMO−6→LUMO and involved electronic density of the C≡CPtC≡C π system (HOMO−6) oriented in a perpendicular manner with respect to the π* porphyrin one (LUMO). So, it is anticipated that this contribution (i.e., HOMO−6→LUMO) does not play a major role in the overall intensity of this Soret band.

The oligomers **P1** and **P2**, again exhibiting an averaged number of repetitive units of 5.8 and 3.2, respectively, were investigated. In these cases, the Soret bands are even more red-shifted down to 462 nm (Figure 5) in comparison to those of **M1** and **M2** (and **L1** and **L2**). The lowest energy Q bands are even more red-shifted down to 678 and 676 nm, in comparison with 658 and 658 nm for **M1** and **M2**, respectively.

The fluorescence and excitation spectra for **P1** and **P2** at both 298 and 77 K are shown in Figure 5. Compared to that at 298 K, the luminescence spectra at 77 K are sharper and slightly red-shifted. The fluorescence spectra shift with the nature of the compounds, such as **L1** = **L2** < **M1** = **M2** < **P1** = **P2**, where the shift of the 0−0 peaks may be up to 40−50 nm, indicating that conjugation is preserved through the Pt atom by mixing of the frontier MOs of Pt and ligands.[15,16]

During the course of this investigation, an upper-energy phosphorescence was noted in the 400−550 nm region for **M1** at 77 K (Figure 6). This luminescence is long-lived (~32 μs; i.e., phosphorescence), and the spectrum bears a strong resemblance to that of *trans*-Pt(P-*n*-$Bu_3)_2(C{\equiv}CC_6H_5)_2$, a unit (under the form of *trans*-Pt(P-*n*-$Bu_3)_2(C{\equiv}C$-*p*-$C_6H_4)_2$ = [Pt]) being part of oligomers or polymers of the type $([Pt]-Ar)_n$ where Ar = M**P**,[12] $C_6X_4N_2$ (X = Cl, OCH_3, CH_3).[17] The excitation wavelength necessary to observe this emission is about 350 nm, and the Soret band is not visible in the absorption spectra, confirming that this emission belongs to the [Pt] unit (−PtL_2CCPh) that is specific to **M1** and **M2**. However, this emission was not seen in **M2**. We have no explanation for this absence of the upper energy luminescence in this case.

In this work, it was not possible to investigate the phosphorescence properties of the porphyrin M**P** units in these materials. In our previous work,[12b] no phosphorescence of the M**P** chromophore was observed except for rare cases such as polymer 9 (Chart 1). In that case, polymer 9 exhibits a phosphorescence 0−0 peak at ~790 nm

(15) Rogers, J. E.; Cooper, T. M.; Fleitz, P. A.; Glass, D. J.; McLean, D. G. *J. Phys. Chem. A* **2002**, *106*, 10108–10115.
(16) (a) Wilson, J. S.; Dhoot, A. S.; Seeley, A. J. A. B.; Khan, M. S.; Köhler, A.; Friend, R. H. *Nature* **2001**, *413*, 828–831. (b) Beljonne, D.; Wittmann, H. F.; Köhler, A.; Graham, S.; Younus, M.; Lewis, J.; Raithby, P. R.; Khan, M. S.; Friend, R. H.; Brédas, J.-L. *J. Chem. Phys.* **1996**, *105*, 3868–3877.
(17) (a) Fortin, D.; Clément, S.; Gagnon, K.; Bérubé, J.-F.; Harvey, P. D. *Inorg. Chem.* **2009**, *48*, 446–454. (b) Gagnon, K.; Aly, S. M.; Fortin, D.; Abd-El-Aziz, A. S.; Harvey, P. D. *J. Inorg. Organomet. Poly. Mat.* **2009**, *19*, 28–34. (c) Gagnon, K.; Aly, S. M.; Brisach-Wittmeyer, A.; Bellows, D.; Bérubé, J.-F.; Caron, L.; Abd-El-Aziz, A. S.; Fortin, D.; Harvey, P. D. *Organometallics* **2008**, *27*, 2201–2214.

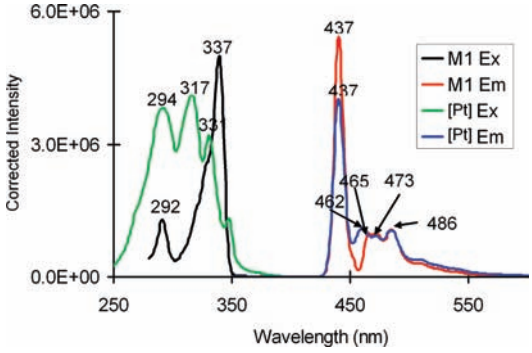

Figure 6. Comparison of the emission (Em, λ_{exc} = 337 nm) and excitation (Ex, λ_{emi} = 437 nm) spectra of **M1** and [Pt] (*trans*-Pt(P-*n*-Bu_3)$_2$-(C≡CC_6H_5)$_2$).

(~12 658 cm^{-1}) and a fluorescence 0−0 signal at ~605 nm (~16 529 cm^{-1}), hence giving an S_1-T_1 gap of ~3870 cm^{-1}. By transferring this value to **M1**, **M2**, **P1**, and **P2**, one would expect this 0−0 peak of phosphorescence in the 900 to 950 nm region. Our detector is sensitive down to 850 nm. Moreover, no long-lived signal was detected in this 850 nm region.

We also attempted to calculate the position of the 0−0 peaks of the phosphorescence (λ_{Phos}) of the M**P** units using DFT by estimating the S_0-T_1 gaps. Both geometries in the S_0 and T_1 states for **L1**, **M1**, and **M2** were performed using the 3-21G*, 6-31G*, and 6-31G* sets supplemented by a THF solvent field (6-31G*/THF), and the S_0, T_1, and S_0-T_1 energies are thus calculated (Table 4). The resulting calculated λ_{Phos} red shifts going from 3-21G* to 6-31G* to 6-31G*/THF for **L1** by a δ of 12 and 18 nm, placing the 0−0 peak at 875 nm in the latter basis sets. Similar conclusions are drawn for **M1** and **M2**, which indicate that the phosphorescence is placed at >850 nm. If one also considers the discrepancy between the computations and the experimental data discussed above for the Q bands (computations are blue-shifted by about 60−80 nm), then the expected position of the 0−0 phosphorescence peak will most likely fall in the 930 nm region. This is consistent with the experimental considerations stated above.

Emisson Lifetimes and Quantum Yields. The fluorescence lifetimes (τ_F) and quantum yields (Φ_F) are reported in Table 1. The trend for both parameters approximatively follows **L1** ~ **L2** > **M1** ~ **M2** ~ **P1** ~ **P2**, which is a predictable consequence of the heavy atom effect induced by the Pt atom (**L1** and **L2** versus **M1**, **M2**, **P1**, and **P2**) where a decrease by about an order of magnitude is noted. Interestingly, both τ_F and Φ_F turned out to be only slightly affected for the Pt-containing materials. A closer look at the data of Table 1 indicates that both τ_F and Φ_F are shorter for **L2**, **M2**, and **P2** in comparison with **L1**, **M1**, and **P1**, respectively, most likely reflecting a loose bolt effect induced by the addition of flexible side chains ($OC_{16}H_{33}$). We also find that both τ_F and Φ_F follow an approximate trend of ligand < model < oligomer. This observation probably reflects the same effect mentioned above: as the number of flexible chains increases, both τ_F and Φ_F decrease. The unexpectedly large decrease in τ_F (~5 fold) and Φ_F (~10 fold) for **M2** at 77 K from 298 K is still unexplained.

Comparison of the Photophysical Properties with Other Pt-Acetylide/Porphyrin Oligomers. New oligomeric species of conjugated metal porphyrin−platinum(II) ethynyl units were prepared and analyzed from a spectroscopic, DFT/TDDFT, and photophysical point of view. Previously, *etio*-porphyrins systems (where the β positions are occupied by CH_3 and CH_2CH_3 groups, and the *meso* positions remain unsubstituted) were reported but were not investigated for photophysical purposes. Upon conjugation through the organometallic unit *trans*-Pt(PBu_3)$_2$, the absorption band shifted down to 676−678 nm, which is a good wavelength for photovoltaic applications.

Table 4. Calculated Position of the Phosphorescence 0−0 peaks for **L1**, **M1**, and **M2**

cpd.	basis sets	$E(S_0)$/a.u.[a]	$E(T_1)$/a.u.[a]	$\Delta E(S_0 - T_1)$/a.u.	λ_{Phos}/nm
L1	3-21G*	−3598.8122	−3598.7580	0.0540	841
L1	6-31G*	−3617.8760	−3617.8226	0.0534	853
L1	6-31G*/THF	−3617.8902	−3617.8381	0.0521	875
M1	6-31G*	−7691.1800	−7691.1272	0.0528	863
M2	6-31G*	−8139.9028	−8139.8497	0.0531	857

[a] From optimized geometries in the S_0 and T_1 states using 6-31G* or 3-21G* basis sets for Zn, C, H, and N; polarized basis sets for P; and SBKJC and VDZ with effective core potentials for Pt.

Two points were raised in this work. The first one is that there is a major change in photophysical properties (τ_F and Φ_F) when the size of the conjugated oligomers and polymers increases. To answer this question, molecules of nanometer dimensions must be examined, such as those presented here (a repetitive unit is on the order of 1.61 nm, the distance between two Pt atoms in **M1**). So **M1** is of 2 nm dimensions and **P1** is about 7.2 nm. The answer to this question is that only slightly perturbed parameters are observed where a small decrease in τ_F and Φ_F is noted. This means that for photovoltaic applications, as the oligomer or the polymer gets longer, nonradiative processes get only slightly more efficient, and so the antenna effect (more specifically energy delocalizations and energy transfers across the materials) is not drastically reduced. On the other hand, as the dimension increases, the extent of energy migration should increase without a major loss of excitation through nonradiative processes such as internal conversion and intersystem crossing.

The second point is, how can we find the difference or confidently assign a decrease in photophysical parameters to either internal conversion (from the singlet and triplet) vs energy transfer? The conjugated molecules and oligomers investigated in this work were selected purposely as they are approximately of the same dimension as the model compound **8** and oligomers **10** (Chart 1) and they are fully conjugated. The full conjugation makes each oligomer practically a distinct molecule with no possibility of intramolecular energy transfer. The oligomer **10**, which was investigated under the form of n = 3, 6, and 9, exhibits two distinct chromophores (*trans*-Pt(P-*n*-Bu_3)$_2$(C≡C-*p*-C_6H_4)$_2$ as [Pt], and M**P**) readily depicted from their respective luminescences. The rates for T_1 energy transfer, k_{ET}, from [Pt] (*trans*-Pt(P-*n*-Bu_3)$_2$(C≡C-*p*-C_6H_4)$_2$) as the energy donor to M**P** as the acceptor, and measured from the decrease in phosphorescence lifetimes, τ_P, of the [Pt] (in comparison with *trans*-Pt(P-*n*-Bu_3)$_2$-(C≡CC_6H_5)$_2$ a model compound) varied from on the order of 10^3 to 10^4 to 10^5 s^{-1} for n = 3, 6, and 9, respectively. The model compound in this case (compound **8** in

Chart 1 for example) exhibits a rate slightly smaller than that for polymer **10** ($n = 3$) perfectly consistent with the change in oligomer dimension. The interpretation of this photophysical event is the presence of an exciton process that delocalizes the excitation energy over the oligomer despite the lesser conjugated $(A-B)_n$ nature of the material. The T_1 k_{ET} gets faster as the extent of delocalization becomes longer. In this work, no energy transfer is possible, and the observed effect is just a modest decrease of the emission lifetimes. This is particularly apparent when comparing **M1** (1 unit) with **P1** (~6 units) at 298 K. One would expect 2 orders of magnitude of variation based on the trend indicated for monomer **8** and polymer **10** ($n = 6$).

Conclusion

The conjugated oligomers **P1** and **P2** exhibit intense and red-shifted Soret and Q-bands. In a situation of a photoinduced electron transfer from the fully conjugated polymer to an added electron acceptor (such as C_{60} for example), the polymer will become cationic, a positive charge that would be delocalized along the backbone. This behavior combined with the strong absorptivity of two bands placed in the visible region of the spectrum (Soret and Q-band) would make the polymers potential materials for photovoltaic applications. In comparison with **L1** and **L2**, there is no drastic decrease in photophysical parameters (factor going from 2 to 3 from Table 1), meaning that there is a minimal decrease in the potential efficiency in the antenna effect (i.e., capturing and migrating the excitation energy across the material) as the rate for nonradiative deactivation is not expected to increase drastically. These oligomers should indeed be examined for photovoltaic performances in order to confirm this in the near future. Moreover, these conjugated oligomers were selected because they acted as distinct molecules where no energy transfer could occur. The conclusion drawn from the photophysical analysis for the 6 compounds investigated is that one can now separate the effect of the oligomer dimension on the photophysical parameters from the stronger influence of the exciton process and energy transfers on them.

Experimental Section

Materials. All reactions were carried out under an argon atmosphere by using standard Schlenk techniques. Solvents were dried and distilled from appropriate drying agents under an inert atmosphere prior to use. Glassware was oven-dried at about 120 °C. All reagents and chemicals, unless otherwise stated, were purchased from commercial sources and used without further purification. Zn(II)(5,15-bis(mesityl)-10,20-bis-(ethynyl)porphyrinate) (**L1**),[8a] Zn(II)(5,15-bis[3,4,5-tri(hexadecyloxy)phenyl]-10,20-bis(ethynyl)porphyrinate) (**L2**),[6j] *trans*-chloro(ethynylbenzene)bis(tri*n*-butyl-phosphine)platinum(II),[18] and *trans*-[Pt(P-*n*-$Bu_3)_2Cl_2$][19] were prepared according to the literature methods.

Zn(II){5,15-bis(mesityl)-10,20-bis[2-(ethynylbenzene)bis(tri-*n*-butylphosphine)platinum(II)-ethynyl]porphyrin} (**M1**) **L1** (50 mg, 0.076 mmol) was reacted with *trans*-chloro-(ethynylbenzene)bis(tri*n*-butyl-phosphine)platinum(II) (113 mg, 0.153 mmol) in cosolvent $iPr_2NH-CH_2Cl_2$ (80 mL, 1:1, v/v) in the presence of CuI (2 mg, 0.010 mmol) for 12 h at room temperature under argon. The solvents were removed with an evaporator under low pressure. The solid was dissolved in minimum dichloromethane and purified by column chromatography on silica gel using dichlormethane/hexane (1:1, v/v) as an eluent. **M1** was obtained in 44% yield. ^{1}H NMR ($CDCl_3$, 400 MHz): δ 0.89 (m, 36 H), 1.39−1.46 (m, 24 H), 1.75−1.80 (m, 24 H), 1.87 (s, 12 H), 2.26−2.34 (m, 24 H), 2.66 (s, 6 H), 7.24−7.29 (m, 10 H), 7.38 (d, 4H, J = 10.3 Hz), 8.52 (d, 4H, J = 6.1 Hz), 9.59 (d, 4H, J = 6.1 Hz). ^{31}P NMR ($CDCl_3$, 160 MHz): δ 5.87 ($^1J_{Pt-P}$ = 3100 Hz). MOLDI-TOF MS: 2057.799 (M^+). Elem anal. calcd (%) for $C_{106}H_{148}N_4P_4Pt_2Zn$: C 61.87, H 7.25, N 2.72. Found: C 61.47, H 7.33, N 2.55. IR (ν/cm^{-1}): 2080. TGA: $T_{10\%decomp}$ = 328 °C.

Zn(II){5,15-bis[3,4,5-tri(hexadecyloxy)phenyl]-10,20-bis[2-(ethynylbenzene)bis(tri-*n*-butyl-phosphine)platinum(II)ethynyl]porphyrin} (**M2**). **L2** (200 mg, 0.099 mmol) was reacted with *trans*-chloro(ethynylbenzene)bis(tri-*n*-butyl-phosphine)platinum(II) (148 mg, 0.200 mmol) in cosolvent $iPr_2NH-CH_2Cl_2$ (100 mL, 1:1, v/v) in the presence of CuI (4 mg, 0.020 mmol) for 12 h at room temperature under argon. The solvents were removed with an evaporator under low pressure. The solid was dissolved in minimum dichloromethane and purified by column chromatography on silica gel using dichlormethane/hexane (1:1, v/v) as a eluent. **M2** was obtained in 47% yield. ^{1}H NMR ($CDCl_3$, 400 MHz): δ 0.83−0.93 (m, 54 H), 1.21−1.27 (m, 168 H), 1.37−1.49 (m, 24 H), 1.80−1.88 (m, 24H), 2.28 (m, 24 H), 4.09 (t, 8H, J = 8.5 Hz), 4.30 (t, 4H, J = 8.5 Hz), 7.10−7.30 (m, 10 H), 7.38 (d, 4H, J = 10.3 Hz), 8.80 (d, 4H, J = 6.0 Hz), 9.64 (d, 4H, J = 6.0 Hz). ^{31}P NMR ($CDCl_3$, 160 MHz): δ 5.95 ($^1J_{Pt-P}$ = 3100 Hz). MOLDI-TOF MS: 3414.219 (M^+). Elem anal. calcd (%) for $C_{196}H_{328}N_4P_4Pt_2Zn$: C 68.91, H 9.68, N 1.64. Found: C 68.45, H 10.00, N 1.57. IR (ν/cm^{-1}): 2081. TGA: $T_{10\%decomp}$ = 300 °C.

Poly{Zn(II)[5,15-bis(mesityl)-10-ethynyl-20-(2-trans-bis(tri-*n*-butylphosphine)platinum(II)-ethynyl)]}porphyrin (**P1**). **L1** (50 mg, 0.076 mmol) was reacted with *trans*-[Pt(P-*n*-$Bu_3)_2Cl_2$] (51 mg, 0.076 mmol) in cosolvent $iPr_2NH-CH_2Cl_2$ (80 mL, 1:1, v/v) in the presence of CuI (2 mg, 0.010 mmol) for 12 h at 65 °C under argon. All the volatile compounds were removed under reduced pressure. The residue was redissolved in CH_2Cl_2 and filtered through a short silica column using dichloromethane as an eluent to give a green solution of the polymeric material. After the removal of solvent by a rotary evaporator, the product was then reprecipitated twice from a CH_2Cl_2/MeOH mixture followed by washing with MeOH to afford a green solid in 60% yield. ^{1}H NMR ($CDCl_3$, 400 MHz): δ 0.8−1.0 (m), 1.1−1.5 (m), 1.6−1.7 (broad peak (br)), 1.8−1.9 (m), 2.1−2.3 (br), 2.4 (br), 2.6−2.7 (m), 7.2−7.4 (m), 8.5−8.7 (br), 9.6−9.8 (br). ^{31}P NMR ($CDCl_3$, 160 MHz): δ 7.57 ppm. IR (ν/cm^{-1}): 2081. GPC (THF): M_w = 10487, M_n = 7307, PD = 1.43. TGA: $T_{10\%decomp}$ = 385 °C.

Poly{Zn(II)[5,15-bis(3,4,5-tri(hexadecyloxy)phenyl)-10-ethynyl-20-(2-trans-bis(tri-*n*-butyl-phosphine)platinum(II)ethynyl)porphyrin]} (**P2**). **L2** (70 mg, 0.035 mmol) was reacted with *trans*-[Pt(P-*n*-$Bu_3)_2Cl_2$] (24 mg, 0.035 mmol) in cosolvent $iPr_2NH-CH_2Cl_2$ (80 mL, 1:1, v/v) in the presence of CuI (2 mg, 0.010 mmol) for 12 h at 65 °C under argon. The resulting solution was diluted by 100 mL of CH_2Cl_2 and washed with water three times. The organic layer was collected, and the volatile compounds were removed under reduced pressure. The residue was washed with CH_2Cl_2 thoroughly to remove the starting materials. This resulted in a dark green solid in 62% yield. ^{1}H NMR ($CDCl_3$, 400 MHz): δ 0.8−1.0 (m), 1.1−1.5 (m), 1.7 (br), 1.8−2.0 (br), 2.4 (br), 4.1 (br), 4.3 (br), 7.4−7.5 (br), 8.9 (br), 9.8 (br). ^{31}P NMR ($CDCl_3$, 160 MHz): δ 7.82. IR (ν/cm^{-1}): 2081. GPC (THF): M_w = 11836, M_n = 8349, PD = 1.41. TGA: $T_{10\%decomp}$ = 312 °C.

Instrumentation. Infrared spectra were recorded as powder or THF solutions using a Perkin−Elmer Paragon 1000 PC or Nicolet Magna 550 Series II FTIR spectrometer, using CaF_2 cells with a 0.5 mm path length. NMR spectra were measured in appropriate deuterated solvents on a JEOL EX270 or a Varian Inova 400 MHz FT-NMR spectrometer, with ^{1}H NMR chemical shifts quoted relative to $SiMe_4$, and ^{31}P chemical shifts

(18) Miki, S.; Ohno, T.; Iwasaki, H.; Yoshida, Z. *J. Phys. Org. Chem.* **1988**, *1*, 333.
(19) Kauffman, B.; Teter, L. A.; Huheey, J. E. *Inorg. Synth.* **1963**, *7*, 245.

relative to an 85% H_3PO_4 external standard. Fast-atom bombardment (FAB) mass spectra were recorded on a Finnigan MAT SSQ710 mass spectrometer in *m*-nitrobenzyl alcohol matrices. The molecular weights of the polymers were determined by GPC (HP 1050 series HPLC with visible wavelength and fluorescent detectors) using polystyrene standards and THF as an eluent, and the thermal analyses were performed with the Perkin−Elmer TGA6 thermal analyzer. The UV/vis spectra were recorded on a Hewlett-Packard diode array model 8452 A at Sherbrooke. The emission and excitation spectra were obtained by using a double monochromator Fluorolog 2 instrument from Spex. Fluorescence and phosphorescence lifetimes were measured on a Timemaster Model TM-3/2003 apparatus from PTI. The source was a nitrogen laser with a high-resolution dye laser (fwhm $\approx$ 1.5 ns), and the fluorescence lifetimes were obtained from high-quality decays and deconvolution or distribution lifetime analysis. The uncertainties were about $\pm$40 ps based on multiple measurements.

Quantum Yield Measurements. For room-temperature measurements, all samples were prepared under an inert atmosphere (in a glovebox, $P_{O2} < 20$ ppm) by dissolution of the different compounds in 2-MeTHF using 1 mL quartz cells with septum (298 K) or quartz NMR tubes in liquid nitrogen for 77 K measurements. Three different measurements (i.e., different solutions) were performed for each set of photophysical data (quantum yields, Φ_F). The sample concentrations were chosen to correspond to an absorbance of 0.05 at the excitation wavelength. Each absorbance value was measured five times for better accuracy in the measurements of emission quantum yield (Φ_F). The Φ_F was referenced to tretraphenylporphyrin, H_2TPP ($\Phi_F = 0.11$ in 2-MeTHF at 77 K).[20] The concentration used for the photophysical examination is around 0.1×10^{-6} to 1×10^{-6} M. The quantum efficiency was also checked by measuring absorbance and integrated fluorescence at various concentrations. The results of such measurements are placed in Figure S7 in the SI where the gradient of the curves becomes proportional to the relative quantum yield of the different samples.

X-Ray Crystallography. The crystals were grown by slow evaporation of a mixture of a CH_2Cl_2/MeOH solution at room temperature. One single crystal of $0.10 \times 0.30 \times 0.80$ mm^3 was mounted using a glass fiber at 198(2) K on the goniometer. Data were collected on an Enraf-Nonius CAD-4 automatic diffractometer at the Université de Sherbrooke using ω scans. The DIFRAC[21] program was used for centering, indexing, and data collection. One standard reflection was measured every 100 reflections; no intensity decay was observed during data collection. The data were corrected for absorption by empirical methods based on ψ scans and were reduced with the NRCVAX[22] programs. They were solved using SHELXS-97[23] and refined by full-matrix least-squares on F^2 with SHELXL-97. The nonhydrogen atoms were refined anisotropically. The hydrogen atoms were placed at idealized calculated geometric positions and refined isotropically using a riding model. Disorder on the butyl groups was treated with equal thermal and bond restraints.

Computational Details. Calculations were performed with Gaussian 03, revision C.02[24] at the Université de Sherbrooke with a Mammouth MP supercomputer supported by le Réseau Québécois de Calculs de Haute Performances. The DFT[25−28] and TDDFT[29−31] were calculated using the B3LYP[32−34] method. 6-31G* or 3-21G*[35−40] basis sets were used for Zn, C, H, and N; polarized basis sets for P;[41,42] and SBKJC and VDZ with effective core potentials[43−45] were used for platinum. The calculated absorption spectra and related MO contributions were obtained from the TD-DFT/Singlets output file and gausssum2.1.[46] THF PCM[47] model was used with all the TDDFT calculations to mimic the 2-MeTHF recorded spectra.

Acknowledgment. This research was supported by the Natural Sciences and Engineering Research Council of Canada (NSERC), le Fonds Québécois de la Recherche sur la Nature et les Technologies (FQRNT), and the Centre d'Études des Matériaux Optiques et Photoniques de l'Université de Sherbrooke.

Supporting Information Available: Crystal data and structure refinement for **M1**; comparison of the calculated spectra for **L1** as a function of the basis set and the presence of THF; TDDFT parameters for the first observable electronic transitions for **M2**; comparison of the calculated spectra for **M1** and **M2**; TDDFT parameters for the four first observable electronic transitions for **M1**; TDDFT parameters for the four first observable electronic transitions for **M2**; decay traces for all compounds and polymers investigated in this work; absorption, excitation and emission spectra of **L1** and **L2** in 2-MeTHF at 298 and 77 K; absorption, excitation, and emission spectra of **M1** and **M2** in 2-MeTHF at 298 and 77 K; intergrated fluorescence intensity as a function of the absorbance of the Soret band where all excitations takes place; Cartesian coordinates of the optimized geometry for **L1**, **M1**, and **M2**; X-ray crystallographic files in CIF format. This material is available free of charge via the Internet at http://pubs.acs.org.

(20) Strachan, J. P.; Gentemann, S.; Seth, J.; Kalsbeck, W. A.; Lindsey, J. S.; Holten, D.; Bocian, D. F. *J. Am. Chem. Soc.* **1997**, *119*, 11191.
(21) Flack, H. D.; Blanc, E.; Schwarzenbach, D. *J. Appl. Crystallogr.* **1992**, *25*, 455–459.
(22) Gabe, E. J.; Le Page, Y.; Charland, J.-P.; Lee, F. L.; White, P. S. *J. Appl. Crystallogr.* **1989**, *22*, 384–387.
(23) Sheldrick, G. M. *SHELXS-97*; University of Göttingen: Göttingen, Germany, 1997; release 97−2.
(24) Frisch, M. J. et al. *Gaussian 03*, revision-C.02; Gaussian, Inc.: Wallingford, CT, 2004.
(25) Hohenberg, P.; Kohn, W. *Phys. Rev.* **1964**, *136*, B864–871.
(26) Kohn, W.; Sham, L. *J. Phys. Rev.* **1965**, *140*, A1133–1138.
(27) Salahub, D. R.; Zerner, M. C. *The Challenge of d and f Electrons*; ACS: Washington, DC, 1989.
(28) Parr, R. G.; Yang, W. *Density-functional theory of atoms and molecules*; Oxford Univ. Press: Oxford, 1989.
(29) Stratmann, R. E.; Scuseria, G. E.; Frisch, M. J. *J. Chem. Phys.* **1998**, *109*, 8218–8224.
(30) Bauernschmitt, R.; Ahlrichs, R. *Chem. Phys. Lett.* **1996**, *256*, 454–464.
(31) Casida, M. E.; Jamorski, C.; Casida, K. C.; Salahub, D. R. *J. Chem. Phys.* **1998**, *108*, 4439–4449.
(32) Becke, A. D. *J. Chem. Phys.* **1993**, *98*, 5648–5652.
(33) Lee, C.; Yang, W.; Parr, R. G. *Phys. Rev. B* **1988**, *37*, 785–789.
(34) Miehlich; Savin, A.; Stoll, H.; Preuss, H. *Chem. Phys. Lett.* **1989**, *157*, 200–206.
(35) Binkley, J. S.; Pople, J. A.; Hehre, W. J. *J. Am. Chem. Soc.* **1980**, *102*, 939–947.
(36) Gordon, M. S.; Binkley, J. S.; Pople, J. A.; Pietro, W. J.; Hehre, W. J. *J. Am. Chem. Soc.* **1982**, *104*, 2797–2803.
(37) Pietro, W. J.; Francl, M. M.; Hehre, W. J.; Defrees, D. J.; Pople, J. A.; Binkley, J. S. *J. Am. Chem. Soc.* **1982**, *104*, 5039–5048.
(38) Dobbs, K. D.; Hehre, W. J. *J. Comput. Chem.* **1986**, *7*, 359–378.
(39) Dobbs, K. D.; Hehre, W. J. *J. Comput. Chem.* **1987**, *8*, 861–879.
(40) Dobbs, K. D.; Hehre, W. J. *J. Comput. Chem.* **1987**, *8*, 880–893.
(41) Labello, N. P.; Ferreira, A. M.; Kurtz, H. A. *J. Comput. Chem.* **2005**, *26*, 1464–1471.
(42) Labello, N. P.; Ferreira, A. M.; Kurtz, H. A. *Int. J. Quantum Chem.* **2006**, *106*, 3140–3148.
(43) Stevens, W. J.; Basch, H.; Krauss, M. *J. Chem. Phys.* **1984**, *81*, 6026–6033.
(44) Stevens, W. J.; Krauss, M.; Basch, H.; Jasien, P. G. *Can. J. Chem.* **1992**, *70*, 612–630.
(45) Cundariand, T. R.; Stevens, W. J. *J. Chem. Phys.* **1993**, *98*, 5555–5565.
(46) O'Boyle, N. M.; Tenderholt, A. L.; Langner, K. M. *J. Comput. Chem.* **2008**, *29*, 839–845.
(47) Miertuš, S.; Tomasi *J. Chem. Phys.* **1982**, *65*, 239–242.